A large-amplitude meander of the shelfbreak front during summer south of New England: Observations from the Shelfbreak PRIMER experiment

Glen Gawarkiewicz, Kenneth H. Brink, Frank Bahr, Robert C. Beardsley, Michael Caruso, and James F. Lynch

Woods Hole Oceanographic Institution, Woods Hole, Massachusetts, USA

Ching-Sang Chiu

Naval Postgraduate School, Monterey, California, USA

Received 10 May 2002; revised 9 June 2003; accepted 11 November 2003; published 4 March 2004.

[1] In order to examine spatial and temporal variability of the shelfbreak front during peak stratification, repeated surveys using a towed undulating vehicle (SeaSoar) are used to describe the evolution of shelfbreak frontal structure during 26 July to 1 August 1996 south of New England. Spatial correlation (*e*-folding) scales for the upper 60 m of the water column were generally between 8 and 15 km for temperature, salinity, and velocity. Temporal correlation scales were about 1 day. The frontal variability was dominated by the passage of a westward propagating meander that had a wavelength of 40 km, a propagation speed of 0.11 m s^{-1}, and an amplitude of 15 km (30 km from crest to trough). Along-front geostrophic velocities (referenced to a shipboard acoustic Doppler current profilers) were as large as 0.45 m s^{-1}, although subject to significant along-front variations. The relative vorticity within the jet was large, with a maximum 0.6 of the local value of the Coriolis parameter. Seaward of the front, a small detached eddy consisting of shelf water was present with a diameter of approximately 15 km. Ageostrophic contributions to the velocity field are estimated to be as large as 0.3 m s^{-1} in regions of sharp curvature within the meander. These observations strongly suggest that during at least some time periods, shelfbreak exchange is nonlinear (large Rossby number) and dominated by features on a horizontal scale of order 10 km. *INDEX TERMS:* 4528 Oceanography: Physical: Fronts and jets; 4520 Oceanography: Physical: Eddies and mesoscale processes; 4219 Oceanography: General: Continental shelf processes; 4536 Oceanography: Physical: Hydrography; *KEYWORDS:* shelfbreak front, cross-shelf exchange, frontal dynamics

Citation: Gawarkiewicz, G., K. H. Brink, F. Bahr, R. C. Beardsley, M. Caruso, J. F. Lynch, and C.-S. Chiu (2004), A large-amplitude meander of the shelfbreak front during summer south of New England: Observations from the Shelfbreak PRIMER experiment, *J. Geophys. Res.*, *109*, C03006, doi:10.1029/2002JC001468.

1. Introduction

[2] The shelfbreak front in the Middle Atlantic Bight remains a problematic feature to study. Collections of individual cross-frontal transects reveal considerable variety in the shape of the front, the interleaving of shelf and slope water masses, and possible processes that might be modulating exchange across the front. While there have been numerous studies of the front including long-term moored arrays [e.g., *Houghton et al.*, 1988], intensive hydrographic surveys [e.g., *Garvine et al.*, 1988], and drifter studies [e.g., *Lozier and Gawarkiewicz*, 2001], the difficulty of studying the front is highlighted by the short temporal decorrelation scales (order of days) identified by *Garvine et al.* [1989]. The short temporal scales create a difficult sampling problem in that individual transects show extreme variations in frontal structure over very short time periods [see *Pickart et al.*, 1999], and it is rarely possible to determine which process, or combination of processes, creates the variations in frontal structure. Similarly, the along-shelf scales of variability in the vicinity of the shelfbreak are also a complicating factor. While instability of the shelfbreak front has long been recognized as an important process in creating frontal variability [e.g., *Flagg and Beardsley*, 1978; *Ramp et al.*, 1983; *Gawarkiewicz*, 1991], observations also suggest that offshore forcing due to eddies over the continental slope contributes to frontal variability and cross-frontal exchange. While not focusing on shelfbreak fronts, the recent review of spiral eddies by *Munk et al.* [2000] provides a nice framework for seeing the effect of eddies near fronts and the generation of filamentary structures visible in sunglint photographs taken from space.

0148-0227/04/2002JC001468$09.00

[3] Despite numerous hydrographic surveys and mooring arrays in this region, only a few studies have dealt with correlation scales within the front and ageostrophic flow within the front. The only prior study to consider correlation scales within the front south of New England was *Garvine et al.* [1989], who used drifter trajectories to estimate Lagrangian temporal correlation scales for velocity. A single mooring at the 80 m isobath was also used to estimate the Eulerian temporal correlation scale, but this mooring was located shoreward of the foot of the front and did not measure any of the velocity field associated with a vigorous shelfbreak eddy field immediately offshore. *Houghton et al.* [1988] did not discuss correlation scales for summer, but found that in winter the velocity was coherent over along-shelf scales of at least 75 km in the along-shelf direction because of strong wind forcing. No work to date has examined correlation scales for temperature, salinity and density within the front.

[4] Similarly, few studies have examined ageostrophic flows within the shelfbreak front south of New England. *Pickart et al.* [1999] inferred the effects of curvature on the front by using the gradient wind with an estimate for frontal curvature derived from the sea surface temperature field. They did not resolve the along-shelf variability of the front beneath the surface. *Fratantoni et al.* [2001] did estimate ageostrophic flow within the front due to topographic convergence, but did not resolve any frontal meanders.

[5] The primary goal of this experiment was to resolve the temporal and spatial correlation scales within the front over a one week period in order to examine day to day variability within the fronts, and to determine how frontal variability affected sound propagation between the continental shelf and slope on a daily basis [*Lynch et al.*, 2001].

[6] The paper is organized as follows. A general description of the field program appears in section 2, along with a brief description of the data processing. The decorrelation scales and a brief description of the thermal wind shears appear in section 3. The structure of the frontal meander and the associated salt fluxes are discussed in section 4. The spatial structure of ageostrophic motions due to flow curvature are treated in section 5. Recent stability studies of the front and their relation to the meander scales observed here are discussed in section 6, along with implications of these results for the horizontal scales of shelf/slope exchange. Conclusions are briefly summarized in section 7.

2. Overview and Data Processing

[7] The Shelfbreak PRIMER field program took place during July and August 1996 along the continental shelf and slope south of New England. In addition to the hydrographic observations described here, acoustic measurements [*Lynch et al.*, 2001] and individual transects across the continental slope using traditional CTD casts were also taken [*Pickart et al.*, 1999; *Fratantoni et al.*, 2001]. The internal tides and the generation of internal "solibores" were reported by *Colosi et al.* [2001].

[8] The study area is shown in Figure 1. A bottom-mounted acoustic Doppler current profiler (ADCP) was deployed for 11 days at the 147 m isobath. From 26 July to 1 August, a four-leg grid was surveyed with a SeaSoar, extending from 40.33°N to 39.92°N, a distance of 47 km. The legs were along 71.16°W, 71.04°W, 70.92°W, and 70.79°W, with a 10 km spacing. This sampling plan was motivated by previous estimates of the length and timescales for frontal variability [*Garvine et al.*, 1989]. The grids generally took 12 to 14 hours to occupy. During the night, an abundance of fishing gear precluded crossing the shelfbreak towing SeaSoar. The first two nights, along-slope sections at roughly the 1000 m isobath were occupied (along 39.83°N). However, the remaining nights were spent in shallow waters. Six complete grids were sampled, and on the final day only the two easternmost transects were completed.

[9] The SeaSoar was towed through the water at a speed of about 8 knots. The vehicle typically cycled between depths of 2 and 120 m or 7–10 m above the bottom, whichever was shallower. The primary instrument was a SeaBird 911+ CTD. Comparison of precruise and postcruise sensor calibrations indicate that the accuracy of the instrument is 0.001 degrees C in temperature and 0.005 for salinity. Processing of SeaSoar data was similar to that described by *Gawarkiewicz et al.* [2001]. The data from the CTD were ultimately averaged into two meter bins in the vertical and 6 min in time. This is equivalent to averaging the upward and downward portions of an undulation offshore, on the deepest dives, into a single vertical profile. In shallower water, the temporal averaging was equivalent to averaging two cycles into a single vertical profile. The typical distance between the 6 min averaged profiles was approximately one kilometer, but varied depending on ship speed. These averaged profiles will be referred to as "raw" in the subsequent text to distinguish them from the objectively mapped data. The coordinate system we use is x oriented to the east and y oriented to the north, as the slope topography is aligned in an east-west axis in this region.

[10] Underway velocity measurements were obtained from the 150 kHz narrowband RD Instruments Acoustic Doppler Current Profiler (ADCP) on board the R/V *Endeavor*. The ADCP was configured to collect data in 3 min ensembles using depth bins of 8 meters. A Differential Global Positioning System (GPS) was used for navigation, and raw data were processed with the Common Oceanographic Data Access System (CODAS) [*Firing et al.*, 1995]. The barotropic tides were removed using data from the bottom-mounted ADCP in 147 m of water. The phase was assumed to be constant within the survey region, and the amplitudes of the semidiurnal velocity components (M_2, N_2, and S_2) were scaled by the ratio of the depth at the ADCP divided by the local water depth. The diurnal tidal components (K_1 and O_1) were assumed to have a constant amplitude throughout the study area as they are primarily oriented along isobaths [*Daifuku and Beardsley*, 1983]. The largest component was the M_2 semidiurnal tide, with a maximum amplitude of 0.06 m s^{-1}. The detailed structure of the baroclinic tide is given by *Colosi et al.* [2001].

3. Statistical Properties

3.1. Means

[11] Before discussing the variability within the fields, we will briefly describe the mean frontal structure (Figure 2). Mean sections were computed by averaging raw observations from all four cross-shelf transects from all surveys at a given latitude in 2 km bins. The vertical bin size is 2 m for hydrographic variables and 8 m for the velocities measured

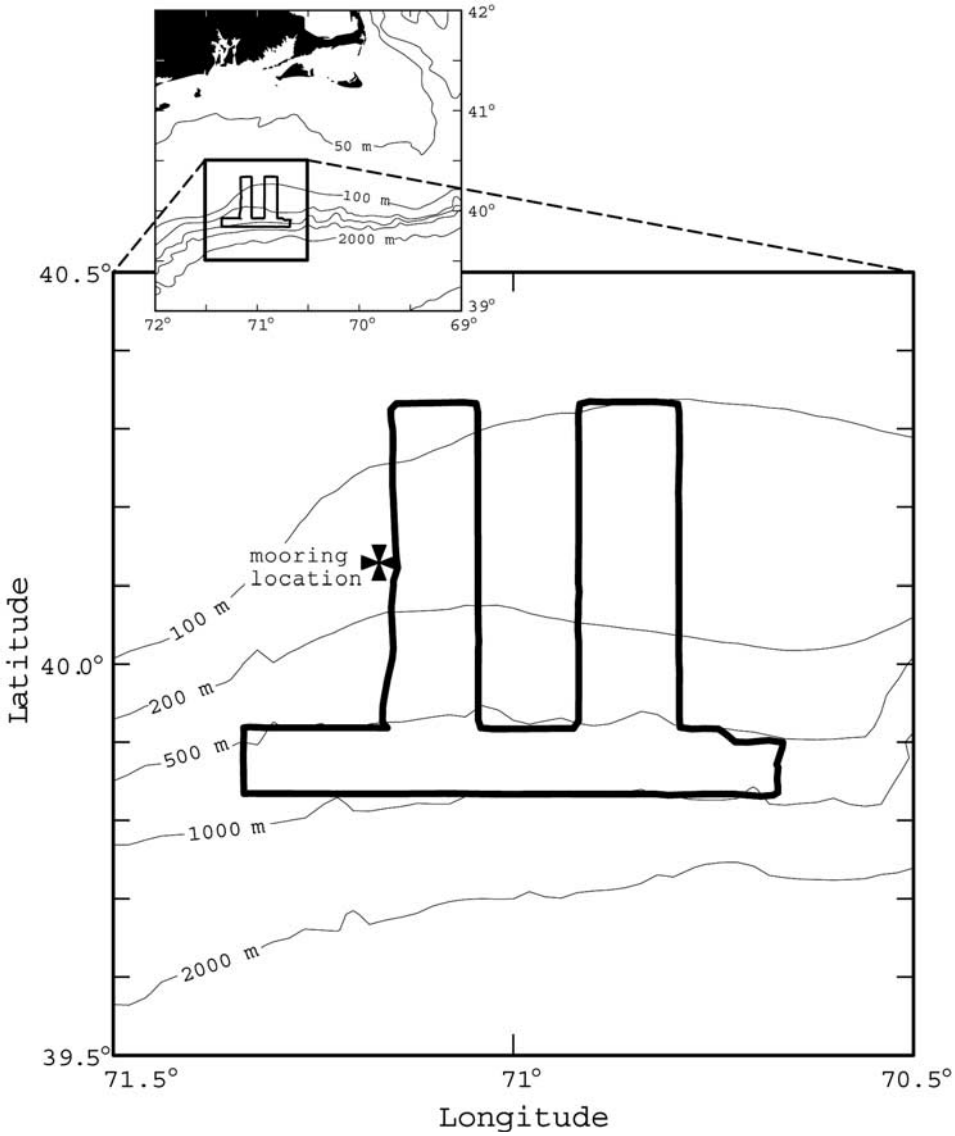

Figure 1. A map of the Shelfbreak PRIMER study region. The general area of the study is denoted by the inset map. The heavy lines denote the SeaSoar track from 26 July 1996. The location of the bottom-mounted ADCP is indicated by the cross. Each of the cross-shelf legs was repeated over 6 days along the same tracks.

by the shipboard ADCP. Since correlation timescales were typically 1 day and the transect spacing was comparable to the spatial correlation scale (see below), each section can usually be treated as independent so there were typically 28 degrees of freedom in each bin.

[12] The mean density structure shows a strong seasonal pycnocline between depths of 10 to 30 m. The density front is predominantly below 40 m depth. The front is more evident in salinity, which increases monotonically offshore. Below 50 m depth, there is a salinity difference of 2.0 across the front (33.0 for shelf water and 35.0 for slope water). The mean along-shelf flow measured by the shipboard ADCP is slightly over 0.2 m s^{-1} to the west, and concentrated in the upper 50 m of the water column at 39.95°N. Mean northward flow is not significantly different than zero over most of the section and so is not presented here.

[13] Salinity variability is greatest within the front (Figure 2b). The maximum standard deviation (0.8) is near the offshore edge of the section at a depth of 40 m, where the cross-shelf gradients are strongest. The maximum variability in density is located within the seasonal pycnocline at a depth of 30 m at 40.1°N, with a maximum standard deviation of 0.4 kg m^{-3}. For the along-shelf velocity, the standard deviations are largest on the shoreward and seaward edges of the mean jet. This pattern is consistent with frontal jet meandering. Thus, in general, the cross-shelf transects captured both the core of the jet and the main structure of the front beneath the seasonal pycnocline, but did not, on average, resolve the surface outcrop of the isohalines.

3.2. Space Scales and Timescales

[14] With an irregularly spaced data set, it is necessary to use objective mapping techniques [e.g., *Bretherton et al.*, 1976] either to display the data set or to create regularly gridded fields to compare one survey to the next. In order to create these objective maps, it is critical to use time and

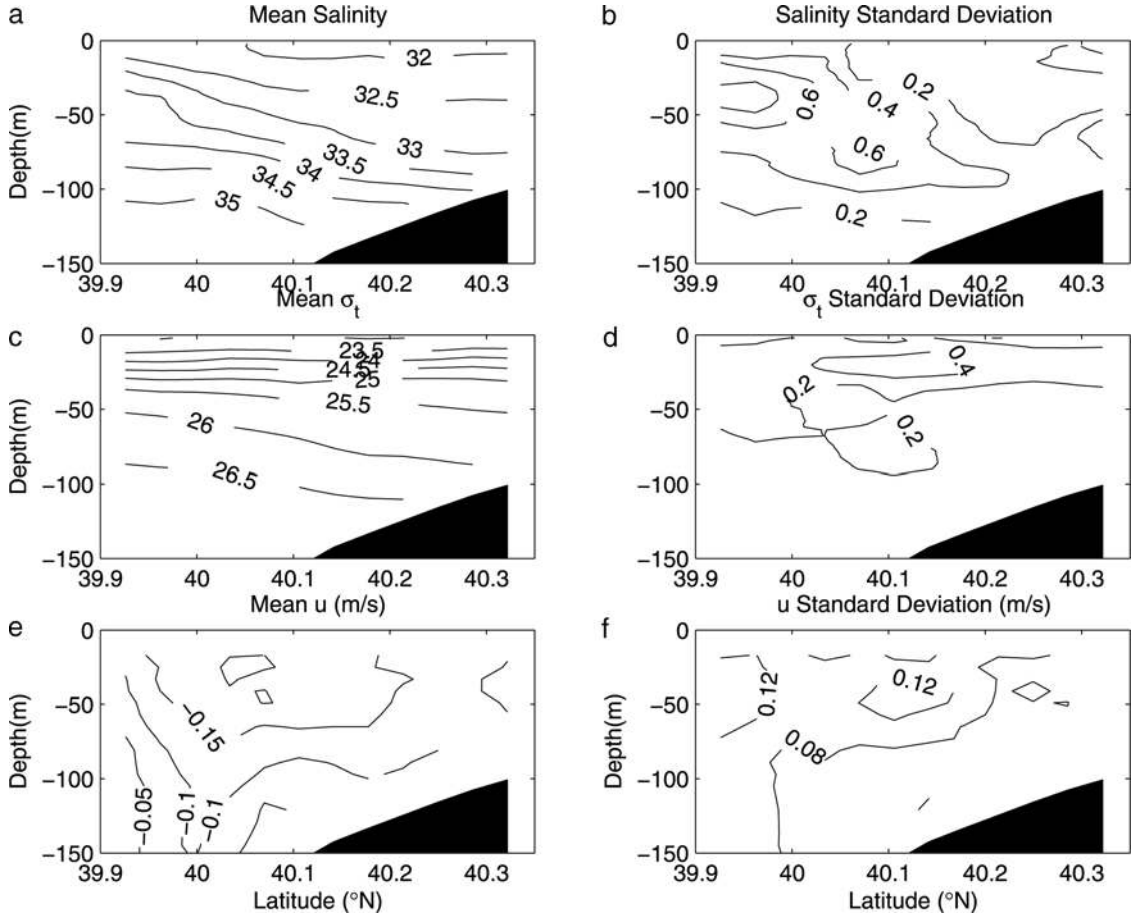

Figure 2. Mean fields of (a) salinity, (c) density, and (e) along-shelf velocity (positive eastward). (b), (d), and (f) Standard deviations of the fields in Figures 2a, 2c, and 2e, respectively. The contour intervals are 0.5 for the mean and 0.2 for the standard deviation of salinity, 0.5 and 0.2 kg m^{-3} for density, and 0.05 m s^{-1} and 0.04 m s^{-1} for along-shelf velocity.

length scales, as well as noise variance estimates, that accurately reflect the data set at hand. The scales also reflect the adequacy of the sampling design for the processes that are present.

[15] For analytical convenience, the space-time autocovariance function C_{qq} for variable q will be approximated by

$$C_{qq} = A_q(1-\epsilon)\cos\Big(\big[(\Delta x/b_x)+(\Delta y/b_y)+(\Delta t/b_t)\big]\cdot \exp\Big[-(\Delta x/a_x)^2-(\Delta y/a_y)^2-(\Delta t/a_t)^2\Big]\Big), \quad (1)$$

where A_q is the variance of the measured q, ϵ is the fraction of this variance that is noise, and a and b are length (x, y) or time (t) scales chosen to fit the observed autocorrelation functions. The scales and noise levels are taken to be different for each variable and at each depth. The scales were calculated by first computing the structure function S_q (binned at typically 0.5 to 1.0 day for time-lagged correlations and 2 km for space-lagged correlations) for separations in x, y, and t (holding the other variables fixed within some tolerance) as, for example,

$$S_q(\Delta x) = N^{-1}\Sigma[q(x)-q(x+\Delta x)]^2, \quad (2)$$

where the sum is over all N pairs of q that are separated by Δx. In computing the spatial structure functions, only samples made within two hours of each other were used for the computations. This avoided any confusion of spatial and temporal correlations.

[16] The temporal structure functions were computed by choosing a sequence of positions (every sixth averaged profile of the first survey) that were generally separated by more than 6 km and that were repeated on each survey. All measurements made within 1 km of these points throughout the 7 day survey period were then found. The values from all of the points were used in the summation of equation (2) to compute the temporal structure function. The structure function is thus representative of the entire sampling region, and a large number of degrees of freedom results.

[17] Once the structure function and variance are known, the autocorrelation function can readily be found. The correlation functions were then fit to equation (1) in order to find the length scales. The noise value ϵ was found by extrapolating the correlation function (which is not computed for zero lag because of the finite bin size for calculating equation (2)) to zero lag, and then taking ϵ to represent the difference between the extrapolation and unity. This approach is consistent with the reasonable assumption that the noise has extremely short scales (much less than 1 day or a few kilometers), and that the signal has longer

Table 1. Correlation Scales

Variable	Depth, m	a_x, km[a]	a_y, km[a]	a_t, days[a]	ε
T	18	7	9	1.5	0.15
T	54	7	7	1.1	0.20
S	18	4	12	1.7	0.20
S	54	7	8	1.1	0.10
ρ	18	8	7	1.4	0.20
ρ	54	20	20	1.1	0.21
u	18	17	12	0.6	0.20
u	41	11	12	0.9	0.10
u	57	9	9	1.0	0.02
v	18	8	9	1.4	0.20
v	41	9	9	0.8	0.09
v	57	12	12	1.0	0.04

[a]Here (a_x, a_y, a_t) = Gaussian length scales in x, y directions and time.

scales. Often, a different value was obtained for the space and time fits. In these cases, the larger value was chosen.

[18] Some representative scales are presented in Table 1. Since the cosine scale b is always much greater (typically 100 days or 100 km) than the exponential scale a, the latter scale is taken to be representative for purposes of the following discussion. We checked our estimates of correlation scales by comparing the residual between the objectively analyzed and raw data to see if the residual was white noise with the correct amplitude. On the basis of these tests, we believe our estimates to be accurate to within 2 km for hydrographic fields and 4 km for velocity. Errors are mainly due to the limited number of realizations. If a larger domain were used, different scales would likely result because of the red spectrum. Similarly, scales oriented along local streamlines might reveal more local anisotropy.

[19] A few results stand out from these calculations.

[20] 1. The timescales a_t are roughly similar for all variables at 54–57 m depth. Near the surface, the scales vary more widely between variables.

[21] 2. Length scales a_x and a_y tend to vary considerably with depth in the water column, as is the case for ρ where spatial scales are much shorter near the surface. Different variables at the same depth tend to have widely varying length scales. This is perhaps intuitive in that we might expect, for example, velocity to have a scale similar to the spatial derivative of density (because of the thermal wind equation), hence shorter than density.

[22] 3. Ideas about two-dimensional turbulence [e.g., *Batchelor*, 1960] would suggest that the correlation scales for velocity ought to be longer in the direction of separation (x direction for u or y direction for v) than in the transverse (y direction for u, x direction for v) direction. This is rarely the case, in that the scales here tend to be isotropic. This is very likely a sampling (insufficient data to obtain high confidence) problem, since the constraint on length scales is quite strong.

[23] 4. One might expect, in coastal regions, to detect a substantial anisotropy, given traditional scalings used for coastal theories [e.g., *Gill and Schumann*, 1974]. The observed correlation scales, however, are strikingly isotropic. Presumably, this relative isotropy is restricted to the area near to, and offshore of, the shelfbreak. Further, it is possible that scale estimates made using larger sampling domains might become more anisotropic. It appears sufficient, however, to note that the variables are relatively isotropic in this area. One implication of this lack of a preferred direction, however, is that it implies that there is no justification to treating shelfbreak structures as two dimensional (y, z) (as has been done until the recent past), since two dimensionality would imply infinite correlation scales in the alongshore direction. Alongshore variability is thus important at lowest order. This conclusion is confirmed by estimates of along-shelf and cross-shelf convergence, and of density advection components (not shown): both show a tendency for variance to be isotropic.

[24] The sampling pattern used (e.g., Figure 1) was chosen on the basis of qualitative a priori knowledge about scales near the shelfbreak front [e.g., *Garvine et al.*, 1989]. along-shelf spacing between cross-shelf transects was taken to be 10 km, and the repeat time was planned to be 1 day. In light of the present results, it is worth asking of the sampling was indeed adequate. Since a_t is typically 1 day or longer, the correlation of the signal (as opposed to the total variance, which is greater than the signal variance by a factor of $[1 - \epsilon]^{-1}$]) from 1 day to the next was about 0.37 or greater. It thus seems reasonable to conclude that the signal variance was sampled well enough in time, and that our individual 1 day surveys were each synoptic. This is not to say, however, that the sampling was good enough to estimate time derivatives with confidence, since differencing enhances the noise level. Spatial scales present a different issue, since some quantities such as density at 18 m depth have shorter scales (8 km), while others, such as density at 54 m depth, have longer scales (20 km). From this, one could conclude that density at 18 m is barely well enough sampled to draw a crude map, but that density at 54 m was well enough resolved to compute spatial derivatives with some confidence. What defines adequate sampling, of course, depends on the scientific question which is addressed.

[25] Maps were produced for each survey of the four leg cross-shelf grid shown in Figure 1. The time interval between maps was 24 hours. The method for objective mapping [*Le Traon*, 1990] uses spatial decorrelation scales which may differ in the along-shelf and cross-shelf directions. As a compromise between the shorter (4–12 km) decorrelation scales near the surface versus the larger (7–20 km) scales below 50 m, a value of 12 km was used in both the cross-shelf and along-shelf directions. Error maps of the objective mapping indicate that maximum expected error values within the sampling grid were less than 10 per cent of the total variance from the mapping of individual variables.

3.3. Geostrophic Velocity Estimates

[26] We wish to obtain the geostrophic velocity field within the meander to estimate cross-shelf salt fluxes and also to quantify the ageostrophic velocity due to flow curvature. Previous examination of the velocity field [*Colosi et al.*, 2001] shows that baroclinic tides are large, making direct usage of the shipboard ADCP problematical. The choice of referencing for geostrophic currents is important in shelfbreak regions because of the large changes in water depth over short cross-shelf distances. In order to test the choice of referencing, the detided shipboard ADCP velocities were compared to the low-pass-filtered velocity from the bottom-mounted ADCP (using a second-order Butterworth filter with a half-power point of 36 hours). This comparison thus gives an indication of how well

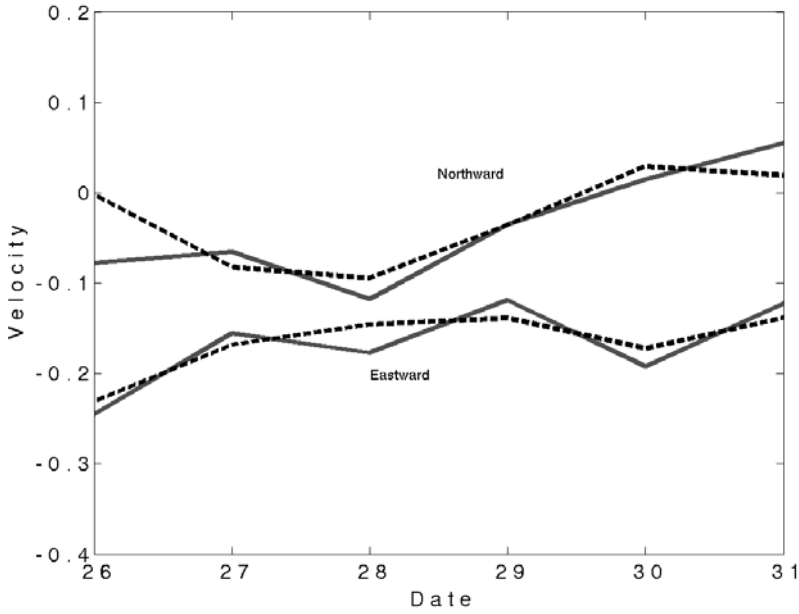

Figure 3. A comparison of the low-pass-filtered northward and eastward velocity components at the bottom-mounted ADCP (dashed line) and from the shipboard ADCP velocities averaged between depths of 40 and 120 m depth for the six times that the ship passed within 2 km of the bottom-mounted ADCP.

instantaneous velocities (measured by the shipboard ADCP) compare to the subtidal motions. At individual 8 m bins, the comparisons were poor, with differences as large as 0.3 m s^{-1}. However, averaging over 40 to 120 m depth resulted in an RMS difference of 0.02 m s^{-1} between the shipboard ADCP and the low-pass-filtered time series from the bottom-mounted ADCP for the six times that the ship passed within 2 km of the moored ADCP (Figure 3). This improvement with vertical averaging is presumably due to the cancellation of the internal tide. Thus, in all referenced geostrophic velocities presented in subsequent sections, the geostrophic velocities are referenced to the shipboard ADCP velocities averaged between 40 and 120 m.

[27] In order to test how well the thermal wind relation held for individual sections, the raw SeaSoar data from individual sections was bin averaged onto a 2 km grid and the density field was then used to compute the thermal wind shear. The cross-shelf sections allow us to compare the vertical velocity shear of the along-shelf current directly with the shipboard ADCP measurements. In general, for individual sections, the comparison between the thermal wind velocity relative to 80 m and the along-shelf (westward) component of the ADCP velocity is poor. While certain sections contained correlations as high as 0.95, other sections even had negative correlations. It will be shown in section 5 that both time dependence and flow curvature are large perturbations to the geostrophic balance within the study region. Simply increasing the spatial bin size to 4 km, but without averaging sections as well (i.e., smoothing only in y but not in x or t) yields only modest improvements in the thermal wind/ADCP agreement.

[28] With sufficient averaging over time and space, the along-shelf flow becomes predominantly geostrophic. Averaging over all 28 sections for both the thermal wind calculation as well as the shipboard ADCP velocity measurements, the regression of thermal wind velocity with the direct measurements using the detided shipboard ADCP is within error of unity. Using a 2 km grid mapping, the correlation between the thermal wind velocity relative to 80 m and the ADCP velocity relative to 80 m was 0.86. The slope of the regression line was 0.76 (i.e., times the thermal wind shear) but well within error of unity. The correlation rises to 0.96 when the density is averaged over 4 km bins in the cross-shelf direction, and the slope of the regression line is 0.95 times the thermal wind shear.

[29] We will present the referenced geostrophic velocities in the following sections. Examination of the vertical shear of the horizontal velocity between 19 m (the shallowest ADCP bin) and 43 m from the bottom-mounted ADCP suggests that the velocity shear was primarily due to the internal tides, so we believe that the referenced geostrophic velocities are more useful for our present purposes. Geostrophic shears in the upper 40 m should still be viewed with caution because of tidal and high-frequency motion of the seasonal pycnocline.

4. Meander Structure and Ageostrophic Velocities

[30] During the study period, the shelfbreak region appears to have been affected by a dipole eddy pair over the continental slope which entrained warm water from the Gulf Stream (Figure 4a). Satellite thermal imagery shows the offshore transport of cool shelf water east of this dipole pair on 21 July. Other images over the following two weeks indicate the presence of relatively warm water over the continental slope which may have originated within the Gulf Stream (Figures 4b, 4c, and 4d). During the SeaSoar observations, the wind stresses were weak, less than 0.1 N m^{-2}. Thus the observations presented here provide a nearly ideal setting for considering frontal structure in the absence of wind forcing.

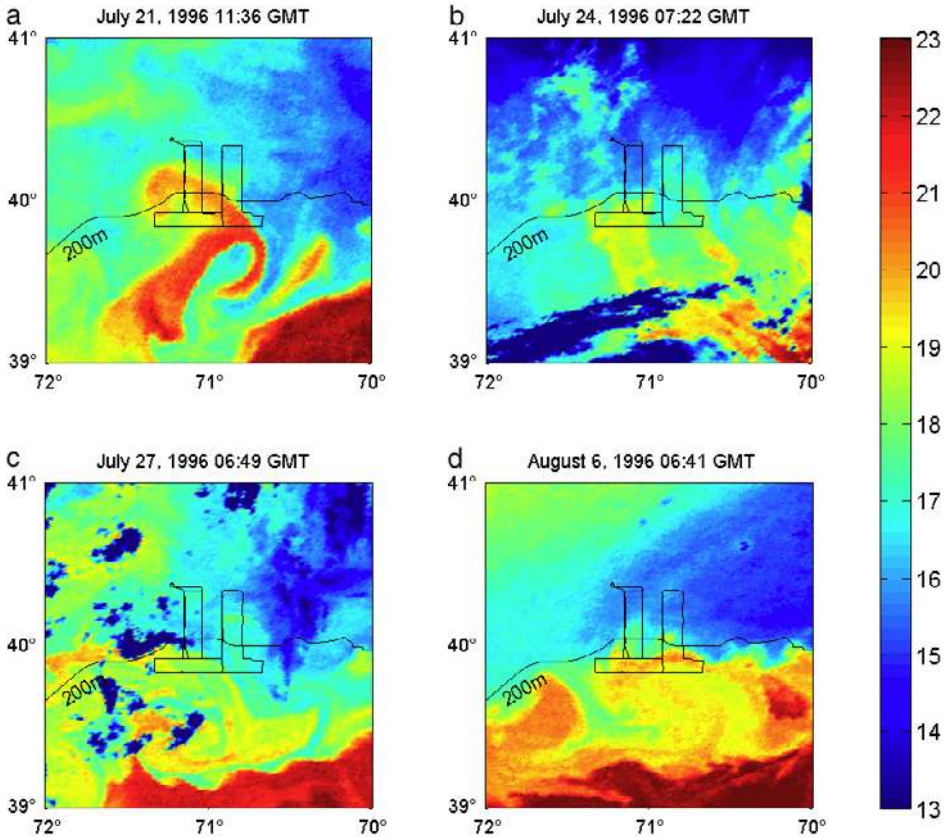

Figure 4. Surface thermal imagery from the study area on (a) 21 July (b) 24 July, (c) 27 July, and (d) 6 August 1996. The color bar on the right indicates the surface temperature in °C. The SeaSoar grid pattern from 26 July is also indicated.

[31] The frontal structure during the SeaSoar observations was dominated by the propagation of a large amplitude meander through the study region. This is most obvious in objective maps of 50 m salinity between 29 and 30 July (Figure 5). Typical cross-frontal density differences were in the range of 0.5 to 0.8 kg m^{-3} (Figure 6). The meander was propagating to the west at 0.11 m s^{-1}. Temperature and salinity fields at selected days (26, 29, and 31 July) reveal several features contributing to shelf-slope exchange associated with the meander (Figures 7 and 8). At the northern edge of the grid on 26 and 27 July, the front is displaced shoreward, and there is a local maximum in temperature (15°C) and salinity (34.5) along the northern boundary. The along-shelf scale for this feature is approximately 16 km. Bottom intrusions of high-salinity water have also been observed by *Lentz et al.* [2003] at the Coastal Mixing and Optics moored array located nearby at the 70 m isobath, as well as by J. Barth (Oregon State University) in his SeaSoar observations later in the summer.

[32] Seaward of the front, a detached eddy of shelf water (minimum temperature of 6°C and minimum salinity of 32.8) is located near 70.9°W and 39.9°N on 26 July. The meander was of large amplitude in the cross-isobath direction relative to the wavelength. The amplitude of the meander was 30 km based on the maximum excursion of the 34.0 isohaline on 29 July. This was comparable to the wavelength which was approximately 40 km.

[33] The cross-shelf structure of the frontal jet varied significantly along the meander. In the trough of the meander (maximum onshore frontal position) the referenced geostrophic flow has two separate areas with strong baroclinic shear; at the foot of the front (near the 100 m isobath) along with a surface-trapped zoned near the surface salinity front outcrop (Figure 9). The maximum velocity near the foot of the front is 0.4 m s^{-1}. The shears above 40 m must be viewed with caution because of the aliasing of the baroclinic tide.

[34] In contrast, the meander crest (maximum offshore frontal position) contains a somewhat weaker jet near the surface (with a maximum along-shelf velocity of 0.25 m s^{-1}; Figure 10). Near the foot of the front, both the isopycnals and isohalines are relatively flat, in strong contrast to the trough of the meander. The strongest jet velocities overall are present at the westernmost section on 26 July (Figure 11). Maximum jet velocities are 0.42 m s^{-1} for the referenced geostrophic velocities. Maximum eastward velocities over the continental slope are as large as 0.3 m s^{-1} (at latitude 39.8°N, not shown in Figure 10), which is presumably induced by the anticyclonic eddy from the vortex pair visible in the thermal imagery.

[35] We will use the gradient wind relationship to look at the influence of the centrifugal force on the development of ageostrophic velocities. Recent work by *Shearman et al.* [2000] and *Watts et al.* [1995] provides a framework for

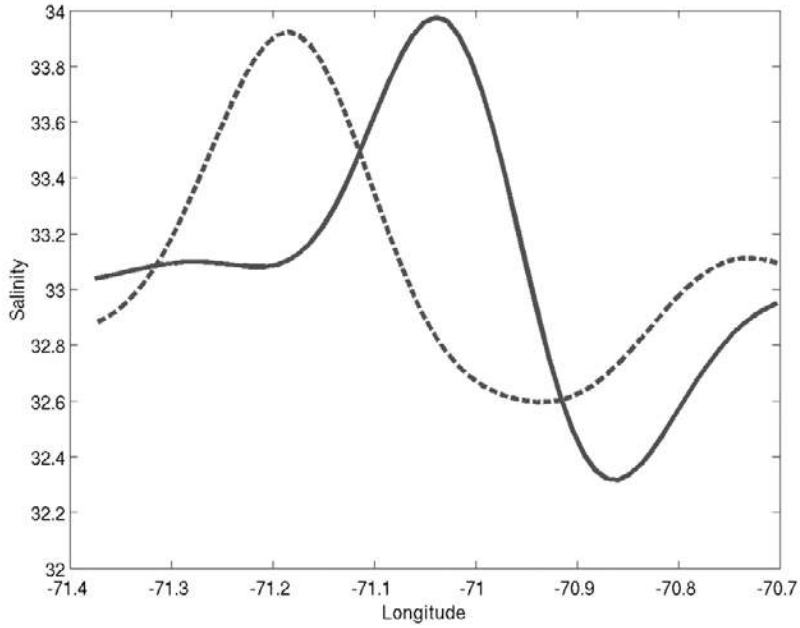

Figure 5. Salinity along 40°N on 29 (solid line) and 30 (dashed line) July, showing the westward propagation of the meander. The westward translation averaged 0.11 m s^{-1} for the 6 days.

investigating the effects of large curvature on ageostrophic flows. The magnitude of inertial effects on the flow within the shelfbreak frontal jet has previously been estimated by *Pickart et al.* [1999].

[36] The gradient wind relationship can be expressed as

$$V^2/R + fV = fV_g, \tag{3}$$

where V is the magnitude of the velocity, or speed, V_g is the

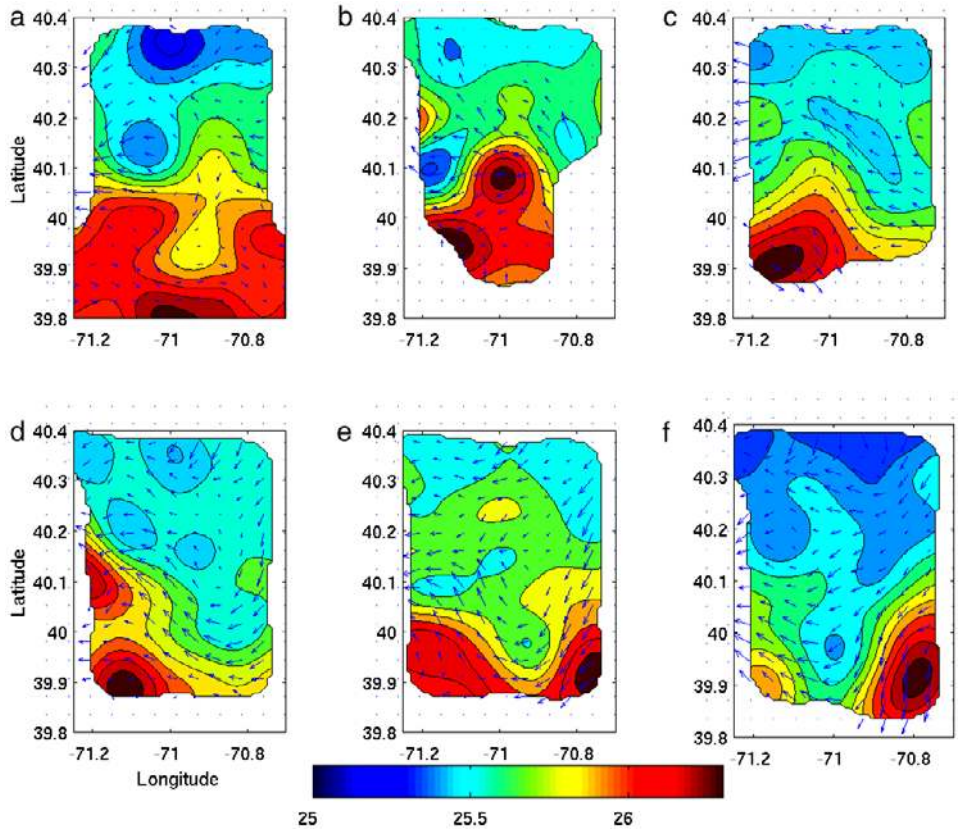

Figure 6. Plan views of the density field at 50 m depth for (a) 26, (b) 27, (c) 28, (d) 29, (e) 30, and (f) 31 July. The contour interval is 0.1 kg m^{-3}. The velocity vectors from the referenced geostrophic field are overlaid.

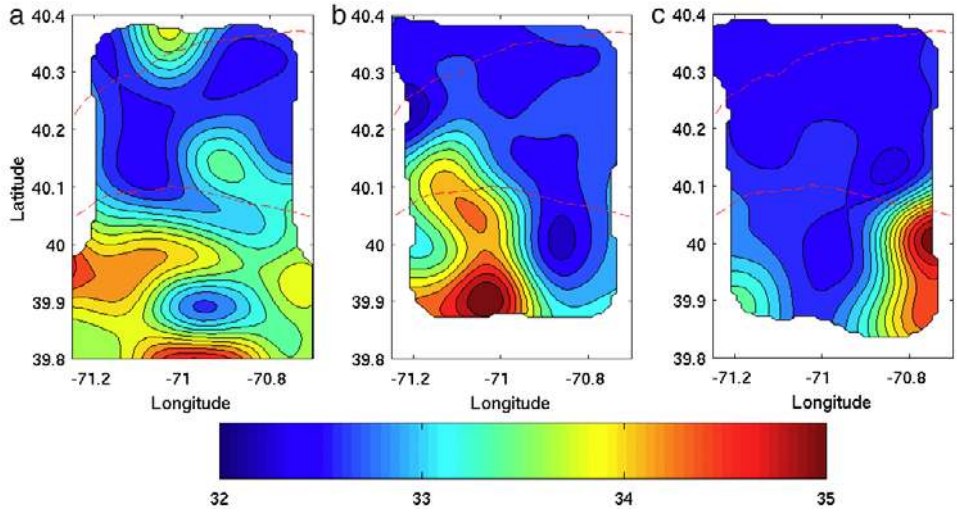

Figure 7. Plan views of the potential temperature field at 50 m depth from (a) 26, (b) 29, and (c) 31 July. The red lines indicate the 100 and 200 m isobaths.

geostrophic velocity, and R is the radius of curvature. If the water parcel trajectories are assumed to be coincident with streamlines in an (assumed) steady state, then the gradient wind velocity V_{gw} is

$$V_{gw} = \frac{2V_g}{1 + (1 + 4\epsilon_R)^{1/2}}. \tag{4}$$

The term ϵ_R is a Rossby number defined as

$$\epsilon_R = \frac{V_g}{fR} \tag{5}$$

with the local radius of curvature defined as

$$R(x,y) = \frac{(u^2 + v^2)^{3/2}}{u^2 v_x - uv(u_x - v_y) - v^2 u_y}. \tag{6}$$

Thus ϵ_R is equivalent to a traditional Rossby number using the radius of curvature as the length scale in the denominator, with the velocities estimated using the referenced geostrophic velocities. The nomenclature is that provided by *Shearman et al.* [2000]. Cyclonic curvature is defined to be positive, and results in gradient wind velocities which are smaller than the geostrophic velocities, while anticyclonic curvature leads to negative values of ϵ_R and thus gradient wind velocities which are larger than the geostrophic values.

[37] The maximum values for the cyclonic (positive) term for ϵ_R is 0.6, while the minimum value (anticyclonic curvature) is -0.4 (Figure 12). The minimum values (hence maximum enhancements of the geostrophic velocities) are associated with the eastern side of the meander crest. This is particularly evident along 39.95°N from 29 to 31 July. The westward propagation of the local minimum is also apparent.

[38] The ageostrophic corrections using the gradient wind relation are a maximum of 0.32 m s^{-1} increase and 0.15 m s^{-1} decrease (Figure 13). The maximum increase occurs on the eastern side of the meander crest. As the meander propagates to the west, the maximum velocity

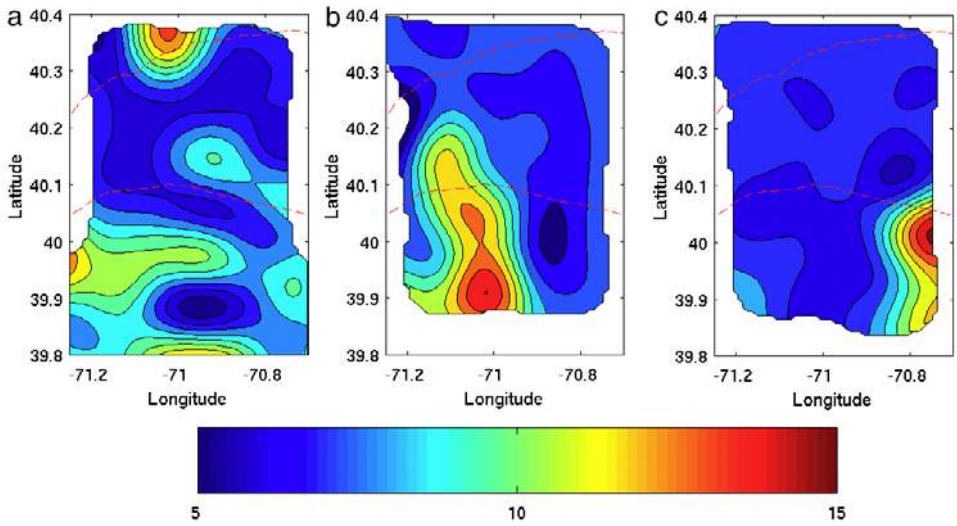

Figure 8. Plan views of the salinity field at 50 m depth from (a) 26, (b) 29, and (c) 31 July.

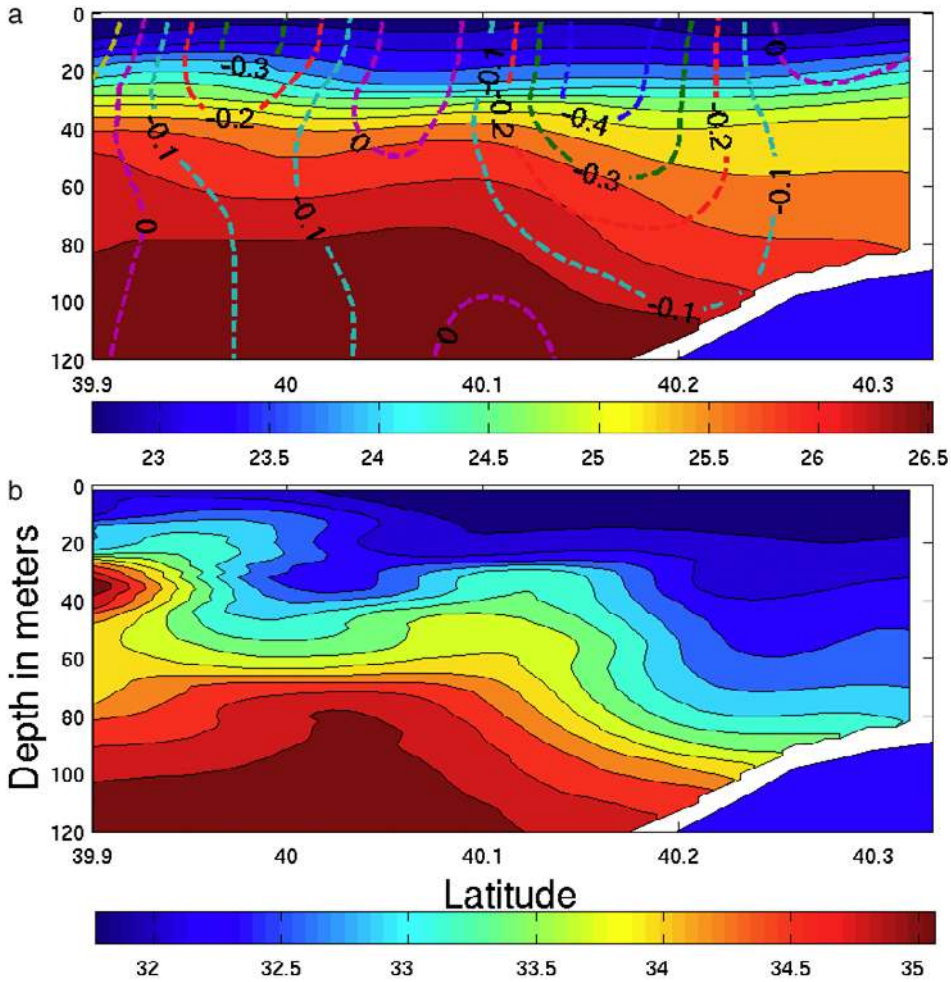

Figure 9. (a) Cross-shelf sections of density and referenced geostrophic velocity from the westernmost section on 29 July. The contour interval for the potential density is 0.5 kg m^{-3} and is 0.1 m s^{-1} for the along-shelf velocity. Negative values for along-shelf velocity denote westward flow. (b) The salinity field from this section with contour intervals of 0.2.

increase along 39.95°N goes from 0.23 m s^{-1} on 29 July to 0.32 m s^{-1} on 31 July. The increase in magnitude is primarily due to an acceleration in the geostrophic velocity as the radius of curvature does not change substantially. Because the temporal evolution is not accounted for the nonlinear modifications must be regarded as first corrections.

[39] In addition to the flow curvature, however, the time dependence is also important. The magnitude of the time derivative of the velocity is shown in Figure 14, where it is scaled by f times the standard deviation of the magnitude of the velocity vector. This is the temporal equivalent of a Rossby number. The time derivative is estimated by finite differencing velocity maps 1 day apart in time. Two maps are shown, between 28–29 July and 30–31 July. For the first case, the maximum nondimensional value is 0.42 near the trough of the meander (y = 40.25°N). This corresponds to a day-to-day difference of 0.41 m s^{-1}. The mean temporal Rossby number over the entire field on this day is 0.19. As the crest propagates through the study region, the maximum value (0.29) shifts offshore to the crest (y = 39.95°N). This corresponds to a maximum day-to-day difference in speed of 0.28 m s^{-1}. For this case, the mean temporal Rossby number over the entire region is 0.15. The standard deviations for the two cases, respectively are 0.11 m s^{-1} and 0.11 m s^{-1}, which correspond to the standard deviation of the speed difference over the entire study region.

[40] Thus, in addition to the nonlinearities from flow curvature, the time dependence is also important and is likely to contribute to the poor comparison between the thermal wind shears and ADCP velocities in the individual sections.

5. Cross-Shelf Fluxes

[41] We will now consider the cross-shelf fluxes of salt both seaward and shoreward of the front. These are not true salt fluxes since they are only across individual sections and do not enclose control volumes (which would remove the need for reference temperature and salinities). To date, the best estimate of fluxes across the shelfbreak front is contained by *Garvine et al.* [1989]. We will initially follow their methodology in order to compare the numbers quantitatively.

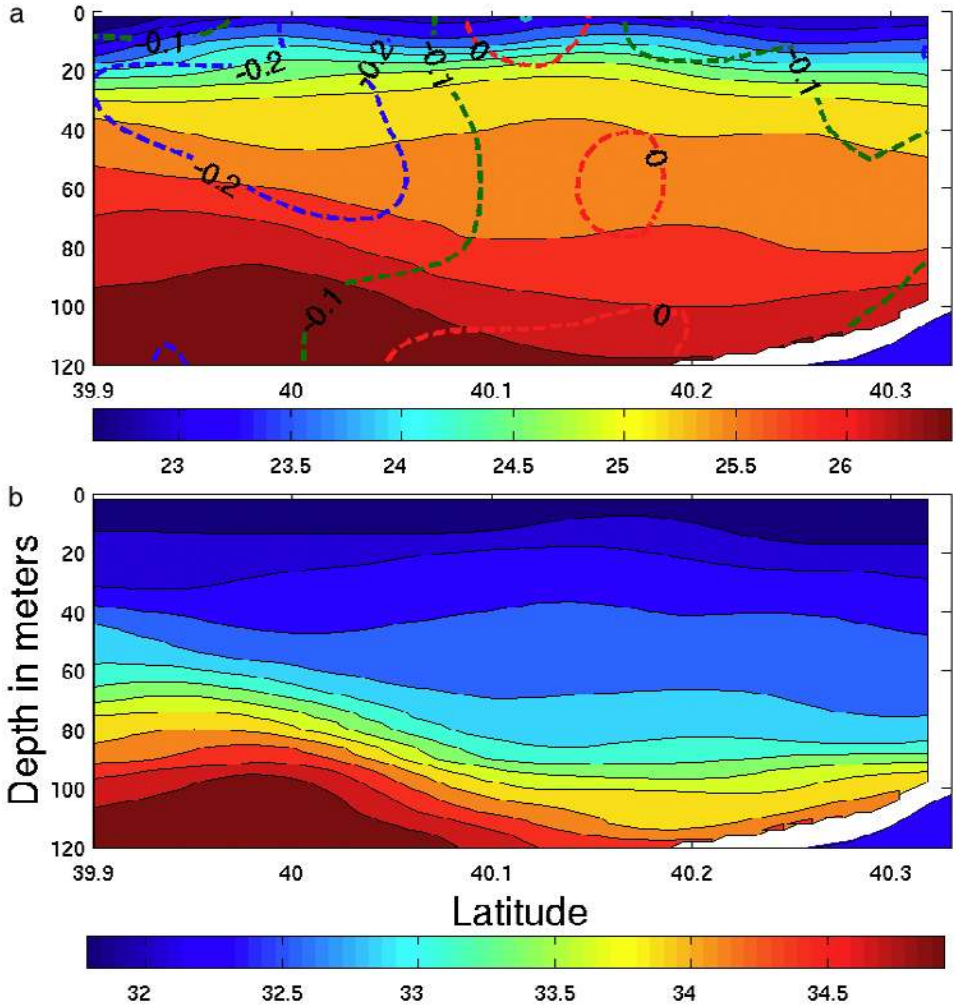

Figure 10. Easternmost section from 29 July showing (a) density and referenced geostrophic velocity and (b) salinity. Contour intervals are the same as in Figure 9.

[42] The flux computation performed by *Garvine et al.* [1989] was

$$F(z) = \frac{1}{\Delta z \Delta x} \int_{z-\frac{\Delta z}{2}}^{z+\frac{\Delta z}{2}} \int_{x_1}^{x_2} \phi(x, z_1) dx dz_1. \quad (7)$$

For F equivalent to the salt flux,

$$\phi = \frac{\rho}{1000}(S - S_m)(v - v_m), \quad (8)$$

where S_m is the mean salinity over the entire section and v_m is the mean cross-shelf velocity. The overall mean salinity from all six sections was 32.45, although different means were used from the sections on each of the 6 days. The horizontal extent was 37.2 km.

[43] The section we will use is the onshore section along 40.33°N, inshore of the typical frontal location. The mean salt flux is onshore (averaged over 6 days) with a value of 0.0067 kg m^{-2} s^{-1}. The range on individual days was between 0.0195 and −0.0018 kg m^{-2} s^{-1} on 26 and 28 July, respectively. The largest values were associated with the near bottom intrusion of warm saline water. The 95 per cent confidence interval for this is 0.0033 kg m^{-2} s^{-1}, so that the onshore salt fluxes are significantly different than zero. (The confidence intervals were computed assuming the degrees of freedom from the total track length over the 6 days).

[44] The salt fluxes were also computed along the slope transect from 26 July (along 39.83°N). This section is about 20 km south of the mean position of the front. The section was 57 km long, and thus had roughly 4 degrees of freedom based on the along-shelf correlation scale of 7 km. The flux was similar in magnitude and was directed onshore, with a value of 0.0072 kg m^{-2} s^{-1}. However, the 95% confidence interval was large compared to this value, 0.035 kg m^{-2} s^{-1}.

[45] The salt fluxes are similar in magnitude to that reported by *Garvine et al.* [1989], who had a value of −0.0048 kg m^{-2} s^{-1}. However, their salt flux was directed offshore. The expected climatological value, based on oxygen isotopes (and quoted by *Garvine et al.* [1989]), is 0.0022 kg m^{-2} s^{-1} onshore, so that the values reported here are roughly three times larger than the climatological value [*Houghton et al.*, 1988; *Fairbanks*, 1982].

[46] The heat flux at the onshore section was also onshore, with a mean value of 0.16 × 10^5 W m^{-2}. The

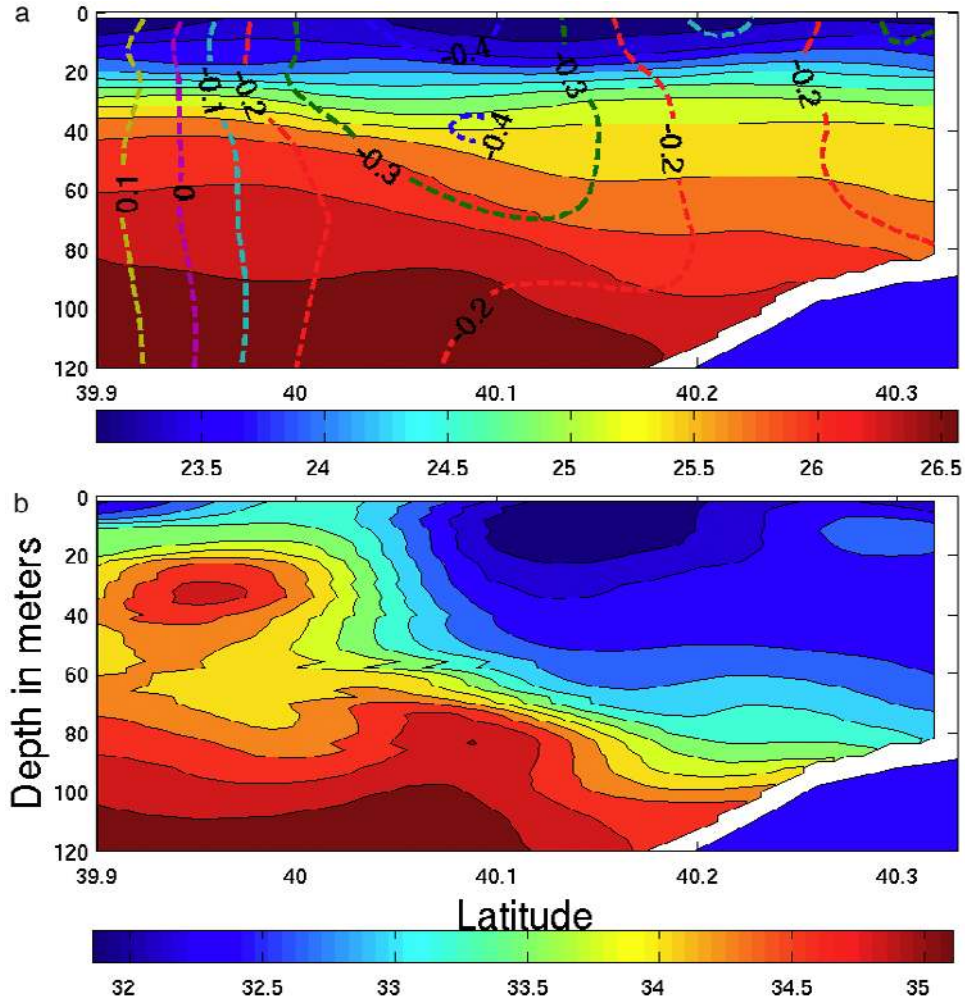

Figure 11. Westernmost section from 26 July showing (a) density and referenced geostrophic velocity and (b) salinity. Contour intervals are the same as in Figure 9.

section average temperature was 9.974 degrees C. The values on individual days ranged between -1.99 and 4.69×10^5 W m^{-2}, with a standard deviation of 2.55×10^5 W m^{-2}. The 95% confidence interval is 1.2×10^5 W m^{-2}, so that the heat fluxes are not significantly different than zero.

[47] The cross-shelf fluxes can also be broken into the more familiar mean and eddy fluxes as a function of cross-shelf position. Using a binning approach similar to that for computing means and standard deviations (section 3), we computed variances and covariances among variables. The covariance of northward velocity v with salinity is then the eddy salinity flux, and this is normalized to compute a correlation. In order to obtain 95% confidence, a correlation magnitude has to reach at least 0.37, although this threshold varies depending on the variable, given the difference in correlation scales. Further, it is also straightforward to compute the product of mean velocity with, say, mean salinity to compute a mean salinity flux.

[48] The northward fluxes associated with the mean flow are not significant at the 95% confidence because the variations in the northward flow are much greater than the mean, so that the mean northward velocity itself is never significantly different than zero. Only a small fraction of the eddy flux estimates are significantly nonzero, and these tend to lie in the upper 40 m near the front. For salinity and temperature, they both represent down-gradient fluxes in the sense of warm, saline slope water moving northward. The density flux is upgradient, in that buoyant water is transported northward, but this is only significant in the upper 30 m where the isopyncnals are relatively flat. This is the opposite of what we would expect from finite amplitude baroclinic instability, but given our inability to compute statistically significant vertically and horizontally integrated fluxes, it is unclear how important the fluxes are above the seasonal pycnocline.

6. Discussion

[49] We will briefly discuss the following implications raised by these observations: horizontal scales of cross-frontal exchange, meander characteristics relative to recent stability studies of shelfbreak fronts, and limitations and difficulties of cross-shelf flux measurements.

6.1. Horizontal Scales of Cross-Shelf Exchange

[50] The observations on 26 July provide an interesting case in which to consider the horizontal scales of cross-shelf exchange. The presence of both a detached eddy seaward of

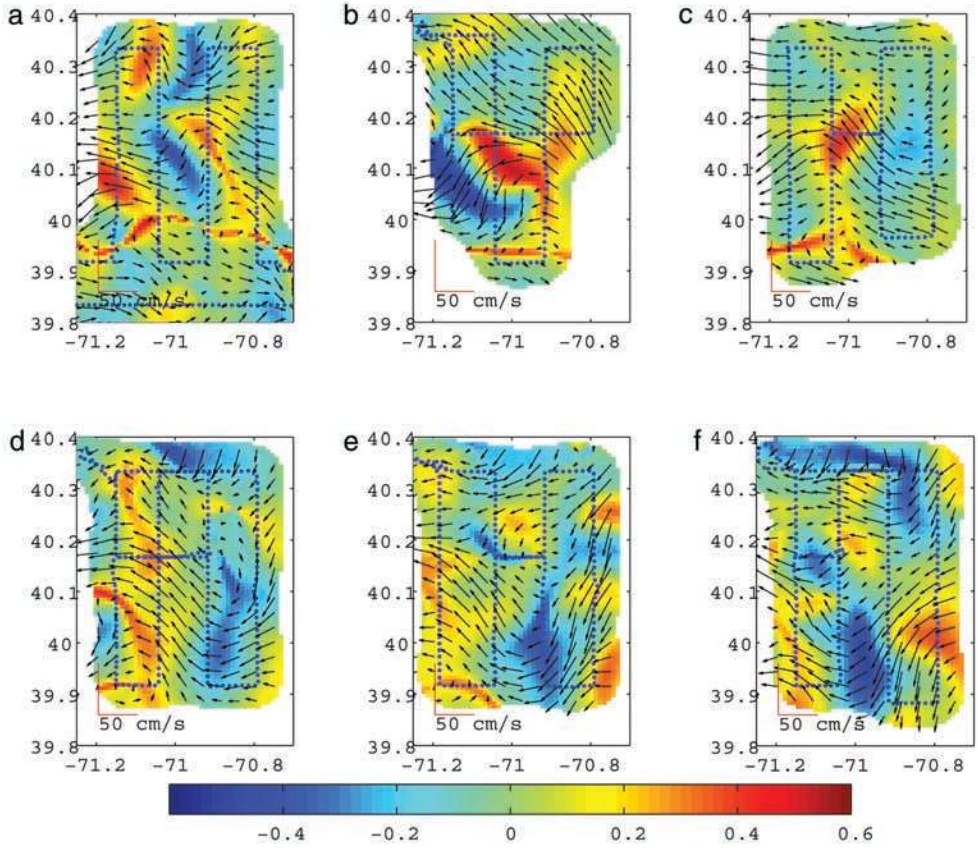

Figure 12. A plan view of ϵ_R at 50 m depth for (a) 26, (b) 27, (c) 28, (d) 29, (e) 30, and (f) 31 July. The color bar indicates the value. The referenced geostrophic velocities are also indicated. Note the band of anticyclonic curvature (blue) translating westward on 29–31 July, with a local extrema near 39.95°N. The dots indicate the locations of the initial raw vertical profiles which went into the objective maps.

the front as well as a bottom-trapped intrusion of slope water onto the continental shelf gives some insight into possible scales over which exchange occurs in the absence of significant wind forcing.

[51] The along-shelf scale of the shelf water eddy is 16 km at a depth of 30 m (using the 33.4 isohaline, which is halfway between the minimum salinity in the eddy and the ambient salinity in the section). The vertical scale of the eddy is approximately 60 m (using the vertical displacement of the 34.0 isohaline).

[52] How does this compare to the baroclinic Rossby radius within the front? During the summertime, there are a number of possible ways to compute the baroclinic Rossby radius. Because of the buoyant water within the surface mixed layer, three different possibilities can be identified [*Gawarkiewicz*, 1991] on the basis of density differences between the surface layer, the shelf water, and the slope water. If we use the density difference between the shelf and slope water as the primary scale, we can define the scale as

$$r_{12} = \sqrt{g'H}/f, \tag{9}$$

where g' is the reduced gravity due to the difference between shelf and slope waters (0.5 kg m^{-3}) divided by the mean density (1025 kg m^{-3}) times g. The vertical scale H is the water depth 100 m, at the foot of the front, and f is the Coriolis parameter (0.94×10^{-4} s^{-1}). This gives a baroclinic Rossby radius of 7.4 km. Thus the eddy radius is comparable to the baroclinic Rossby radius r_{12}.

[53] Similarly, the horizontal scale for the bottom intrusion at 80 m depth is 16 km. The vertical scale of this feature is approximately 40 m (using the 33.5 isohaline). The maximum salinity 10 m above the bottom on the shelf is 34.2. In the horizontal maps of temperature and salinity presented earlier (Figures 7 and 8), this feature occurs at the trough of the meander where the isohalines reach their maximum shoreward extent. Further evidence for the relationship between the meander and the shoreward intrusion of the slope water is the westward propagation of the density anomaly between 26 and 27 July at 10 km day^{-1}, which is roughly the phase speed of the meander. Thus the length scales of the primary features associated with exchange are on scales comparable to the baroclinic Rossby radius.

[54] An interesting aspect of these horizontal scales is their relation to that of spiral eddies observed in sunglint photographs taken from space shuttle missions [*Munk et al.*, 2000]. The spiral eddies horizontal scales (10–25 km), timescales (order 1 day), and relative vorticity (0.3 f, with predominantly cyclonic shear) are all similar to the scales observed here. It is quite possible that the shelfbreak front serves as a significant source for these eddies. We note that Scully Power's sketch of a sheet of vortices south of Long Island [*Munk et al.*, 2000, Figure 35] may very well have

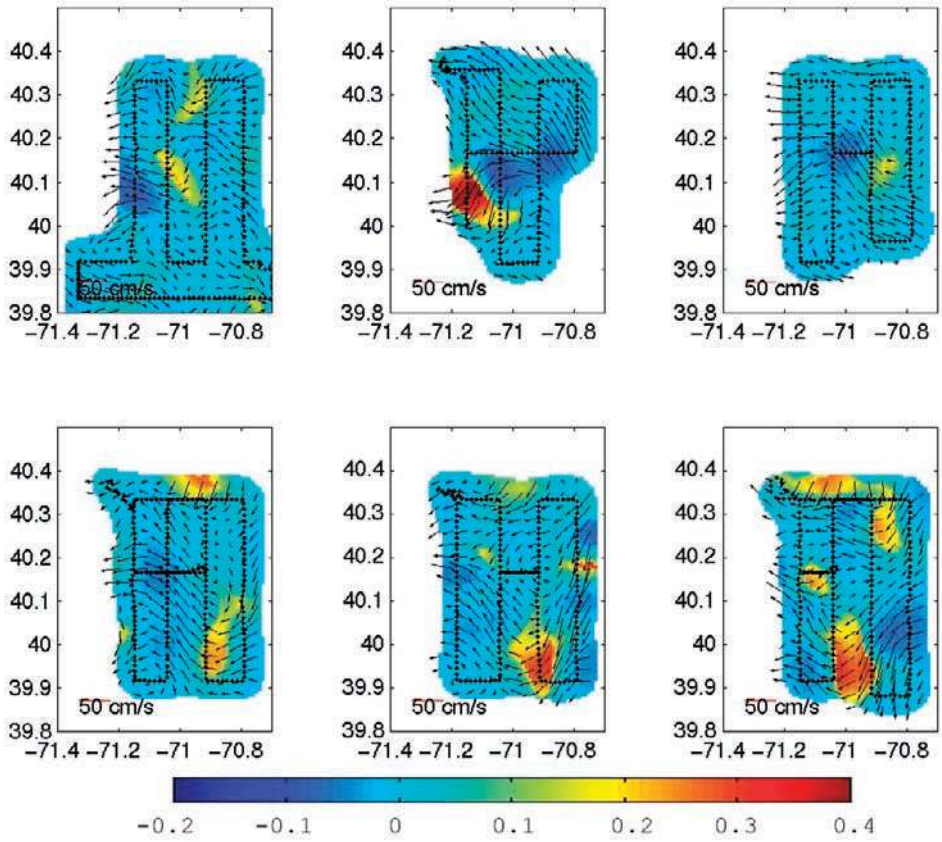

Figure 13. Plan views of the correction for the geostrophic velocities by flow curvature using the gradient wind relation for (a) 26, (b) 27, (c) 28, (d) 29, (e) 30, and (f) 31 July. The color bar indicates the values, which are in m s^{-1}. The largest increases are on the eastern side of the meanders. Note the local minima near 39.95°N on 29–31 July, which propagates westward. The referenced geostrophic velocity vectors are also indicated.

been along the shelfbreak front. Surface thermal imagery [e.g., *Garvine et al.*, 1988, Figure 4] frequently indicates eddies in vortex sheets along the front. However, the Gulf Stream and related features (warm outflows, warm core rings) may also serve as a potential source for spiral eddies.

6.2. Meander Characteristics and Frontal Stability

[55] There have been a number of studies concentrating on the stability of shelfbreak fronts. The most relevant recent studies are *Gawarkiewicz* [1991], who used a model with three homogeneous layers to examine the stability of the front in summer, and *Lozier et al.* [2002], who included continuous vertical and horizontal velocity shears. In general, both models produce unstable waves over a broad range of wavelengths between 10 and 50 km. Thus theoretical studies suggest that the front is potentially unstable at the observed wavelength (40 km), although each of these studies has some limitation in the application to this case.

[56] The three-layer model of *Gawarkiewicz* [1991] was used with a density difference of 0.5 kg m^{-3} across the subsurface front. Shelf and slope water densities were chosen to be 1026.0 and 1026.5 kg m^{-3}, while the surface layer density was chosen to be 1024.0 kg m^{-3}. Using shelf and slope velocities of 0.32 and 0.02 m s^{-1}, respectively, and a bottom slope of 0.005, the most unstable wave at a wavelength of 40 km has a period of 3.4 days and an *e*-folding timescale for growth of 1.86 days. The phase velocity of this wave is 0.15 m s^{-1} to the west, in the direction of the mean flow. The most unstable wave had a wavelength of 35 km. Thus the meander characteristics are consistent with expected scales produced by this simple (infinitesimal amplitude) model.

[57] The more complicated (but still assuming infinitesimal amplitude) model of *Lozier et al.* [2002] uses a background state with continuous stratification so that arbitrary horizontal and vertical velocity shears can be specified in the background state. However, there was no seasonal pycnocline present in their model runs. The closest case used a maximum jet velocity of 0.3 m s^{-1} and had a Rossby number of 0.3. For this case [see *Lozier et al.*, 2002, Figure 10a], phase speeds were between 0.08 and 0.15 m s^{-1} and e-folding timescales for growth were 3–4 days for a wavelength of 40 km. The range of values is due to systematic changes in ambient linear stratification added to the frontal structure. Thus this more complicated model also suggests that frontal instabilities are possible for the observed wavelength.

[58] The wavelength observed here is slightly longer than previously observed. *Garvine et al.* [1988] observed a frontal wave with a wavelength of 33 km in this area, while *Ramp et al.* [1983] used surface thermal imagery to observe a frontal wave with a wavelength of 23 km along the front

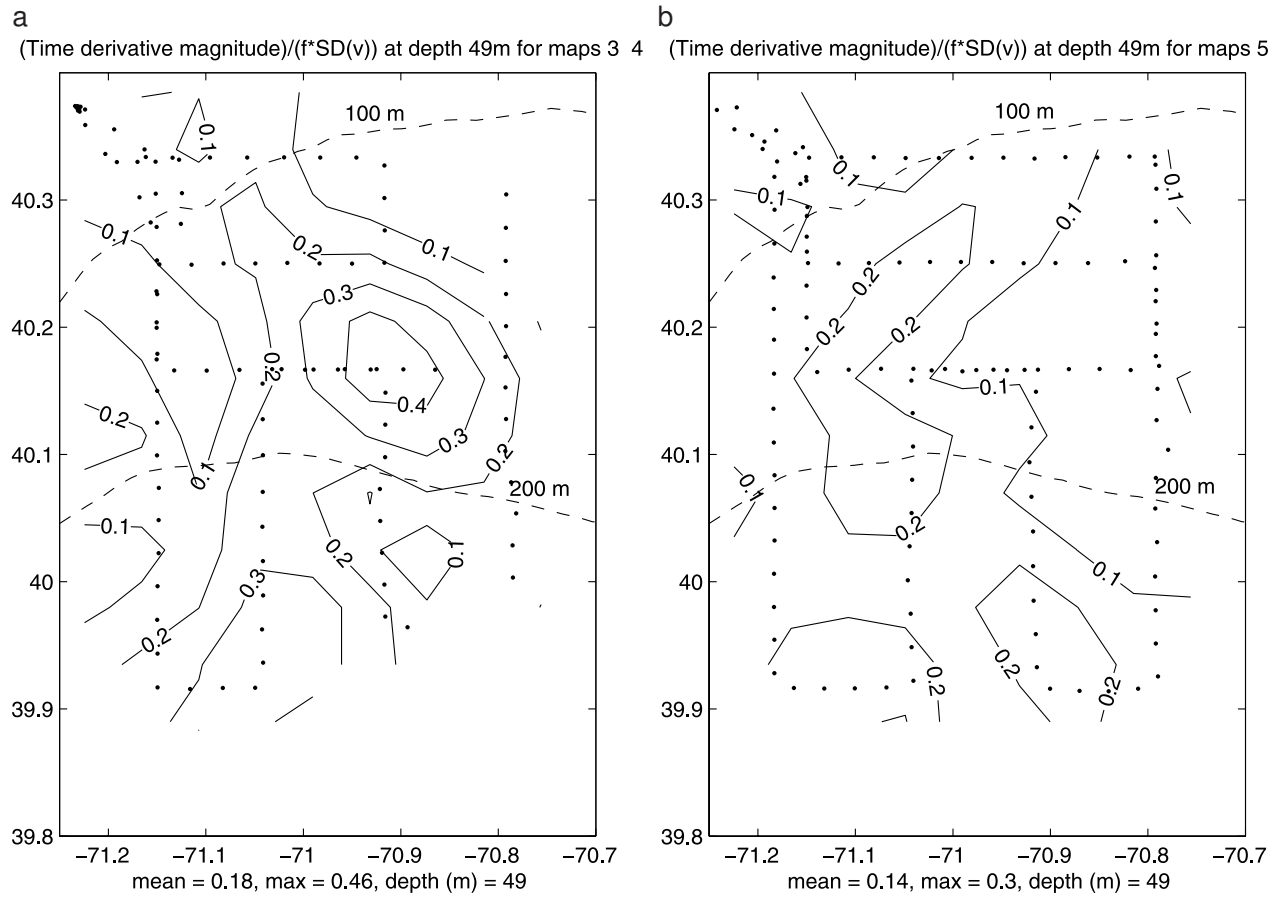

Figure 14. The nondimensionalized magnitude of the time derivative for the velocity vectors between successive days, with (a) 28–29 July and (b) 30–31 July. The derivative is nondimensionalized by f times the standard deviation of the total velocity, which is 0.11 m s^{-1} for the two cases. The dots indicate the locations of the raw vertical profiles that went into the objective mapping.

in the vicinity of a warm-core ring. Both satellite thermal imagery and the theoretical stability studies suggest a wide range of wavelengths is possible for instabilities near the front.

[59] Future work will be necessary to understand how the infinitesimal disturbances progress into large amplitude features. *Lermusiaux* [1999] and *Sloan* [1996] have studied the finite amplitude behavior of shelfbreak frontal meanders using the Harvard Ocean Prediction System and feature models of the front, but further study is necessary in this area.

6.3. Limitations on Observing Cross-Shelf Fluxes

[60] The cross-shelf fluxes of heat and salt presented in the previous section appear to be sensible in magnitude in that they are several times above the climatological values and are of similar magnitude (though not necessarily direction) as *Garvine et al.* [1989]. We will briefly discuss some of the limitations of our measurements.

[61] The primary advantage of the fluxes computed both shoreward and seaward of the front is that the estimates are less noisy because the sections do not intersect the meandering frontal jet. As *Garvine et al.* [1989] note, their net fluxes were an order of magnitude smaller than the fluxes of the individual onshore and offshore components of the frontal meander which they observed. By taking the fluxes seaward of the front, there is less potential aliasing of the along-shelf fluxes. In addition, the Rossby numbers are fairly high relative to the Coriolis parameter and flow curvature can be large, so that the flows near the jet are subject to greater nonlinearity and uncertainty as to the actual velocity.

[62] A big limitation in estimating the fluxes is the large value of the standard deviation of $v'T'$ and $v'S'$ relative to the mean values. In order to reduce the 95 per cent confidence interval seaward of the front (along 39.83°N) to a size comparable to the mean value, the degrees of freedom must be increased by a factor of 25. Assuming that the spatial decorrelation scale is 7 km, this implies that a track length of 1400 km would be necessary. Alternatively, assuming a temporal decorrelation scale of 1 day, 200 days of observations at a single point would be necessary. This highlights the extreme difficulty of obtaining statistically significant cross-slope fluxes over the upper slope. Shoreward of the front, however, the onshore salt flux was significantly different than zero, and was consistent with the value seaward of the front.

7. Conclusions

[63] High-resolution hydrographic observations from the shelfbreak front during July 1996 reveal the passage of a

large-amplitude frontal meander. The meander had a wavelength of 40 km and a peak-to-trough amplitude of 30 km. Jet velocities using referenced geostrophic values were typically 0.3 m s^{-1} with maximum values of 0.45 m s^{-1}. Maximum relative vorticities (with a 12 km spatial smoothing) were as large as 0.6 of the Coriolis parameter. Ageostrophic velocities estimated using the gradient wind relation were as large as 0.3 m s^{-1}, respectively, indicating that flow curvature was important in the frontal dynamics. Estimates of cross-shelf fluxes of salt indicate onshore transport with a value three times larger than expected from climatological values. Important features contributing to cross-shore fluxes included a detached eddy of shelf water present over the upper slope and a near-bottom intrusion of slope water onto the continental shelf. These observations suggest that cross-shelf exchange in the vicinity of the shelfbreak occurs over relatively small space and timescales.

[64] **Acknowledgments.** This work was performed under grants N-00014-95-1-0575 and N-00014-98-1-0059. as part of the ONR Shelfbreak PRIMER Initiative. Some additional analysis and writing was done under ONR grants N-00014-00-1-0931 and N-00014-01-1-0247. We thank the WHOI SeaSoar group, including Paul Fucile, Jerry Dean, Al Gordon, and Craig Marquette, for outstanding work at sea as well as design and implementation of the bottom avoidance system. John Kemp did an outstanding job deploying and recovering the moorings used in this study. The captain and crew of the R/V *Endeavor* provided excellent support throughout the cruise, which involved numerous encounters with a wide variety of fishing gear. We thank the other Shelfbreak PRIMER investigators for support throughout this work. We thank R. Pickart, P. Fratantoni, K. Shearman, and S. Lozier for helpful discussions. S. Ramp, L. Goodman, and J. Simmen of the Office of Naval Research were extremely supportive throughout, and we greatly appreciate their encouragement. W.H.O.I. contribution number 10736.

References

Batchelor, G. K. (1960), *The Theory of Homogeneous Turbulence*, 197 pp., Cambridge Univ. Press, New York.

Bretherton, F., R. Davis, and C. Fandry (1976), A technique for objective analysis and design of oceanographic experiments applied to MODE-73, *Deep Sea Res.*, *23*, 559–582.

Colosi, J., R. Beardsley, J. Lynch, G. Gawarkiewicz, C.-S. Chiu, and A. Scotti (2001), Observations of nonlinear internal waves on the outer New England continental shelf during the summer Shelfbreak PRIMER study, *J. Geophys. Res.*, *106*, 9587–9601.

Daifuku, P., and R. Beardsley (1983), The K_1 tide on the continental shelf from Nova Scotia to Cape Hatteras, *J. Phys. Oceanogr.*, *13*, 3–17.

Fairbanks, R. (1982), The origin of continental shelf and slope water in the New York Bight and Gulf of Maine: Evidence from $H_2^{18}0/H_2^{16}0$ ratio measurements, *J. Geophys. Res.*, *87*, 5796–5808.

Firing, E., J. Ranada, and P. Caldwell (1995), Processing ADCP data with the CODAS Software System, technical report, 218 pp., Univ. of Hawaii, Honolulu.

Flagg, C., and R. Beardsley (1978), On the stability of the shelf-water/slope-water front south of New England, *J. Geophys. Res.*, *83*, 4623–4631.

Fratantoni, P., R. Pickart, D. Torres, and A. Scotti (2001), Mean structure and dynamics of the shelfbreak jet in the Middle Atlantic Bight during fall and winter, *J. Phys. Oceanogr.*, *31*, 2135–2156.

Garvine, R., K.-C. Wong, G. Gawarkiewicz, R. McCarthy, R. Houghton, and F. Aikman III (1988), The morphology of shelfbreak eddies, *J. Geophys. Res.*, *93*, 15,593–15,607.

Garvine, R., K.-C. Wong, and G. Gawarkiewicz (1989), Quantitative properties of shelfbreak eddies, *J. Geophys. Res.*, *94*, 14,475–14,483.

Gawarkiewicz, G. (1991), Linear stability models of shelfbreak fronts, *J. Phys. Oceanogr.*, *21*, 471–488.

Gawarkiewicz, G., F. Bahr, R. Beardsley, and K. Brink (2001), Interaction of a slope eddy with the shelfbreak front in the Middle Atlantic Bight, *J. Phys. Oceanogr.*, *21*, 2783–2796.

Gill, A., and E. Schumann (1974), The generation of long shelf waves by wind, *J. Phys. Oceanogr.*, *4*, 83–90.

Houghton, R. W., F. Aikman III, and H. W. Ou (1988), Shelf-slope frontal structure and cross-shelf exchange at the New England shelfbreak, *Cont. Shelf Res.*, *8*, 687–710.

Le Traon, P. (1990), A method for optimal analysis of fields with spatially variable mean, *J. Geophys. Res.*, *95*, 13,543–13,547.

Lentz, S., K. Shearman, S. Anderson, A. Plueddemann, and J. Edson (2003), Evolution of stratification over the New England shelf during the Coastal Mixing and Optics study, August 1996–June, 1997, *J. Geophys. Res.*, *108*(C1), 3008, doi:10.1029/2001JC001121.

Lermusiaux, P. (1999), Data assimilation via error subspace statistical estimation. Part II: Middle Atlantic Bight shelfbreak front simulations and ESSE validation, *Mon. Weather Rev.*, *127*, 1408–1432.

Lozier, M. S., and G. Gawarkiewicz (2001), Cross-frontal exchange in the Middle Atlantic Bight as evidenced by surface drifters, *J. Phys. Oceanogr.*, *31*, 2498–2510.

Lozier, M. S., M. Reed, and G. Gawarkiewicz (2002), Instability of a shelfbreak front, *J. Phys. Oceanogr.*, *32*, 924–944.

Lynch, J., A. Newhall, B. Sperry, G. Gawarkiewicz, P. Tyack, and C.-S. Chiu (2001), Spatial and temporal variations in acoustic propagation characteristics at the New England shelfbreak front, *IEEE J. Oceanic Eng.*, *28*, 129–150.

Munk, W., L. Armi, K. Fischer, and F. Zachariasen (2000), Spirals on the sea, *Proc. R. Soc. London, Ser. A*, *456*, 1217–1280.

Pickart, R., D. Torres, T. McKee, M. Caruso, and J. Przystup (1999), Diagnosing a meander of the shelfbreak front in the Middle Atlantic Bight, *J. Geophys. Res.*, *104*, 3121–3132.

Ramp, S., R. Beardsley, and R. Legeckis (1983), An observation of frontal wave development on a shelf-slope/warm core ring front near the shelf break south of New England, *J. Geophys.*, *81*, 3695–3708.

Shearman, R. K., J. Barth, J. Allen, and R. Haney (2000), Diagnosis of the three-dimensional circulation in mesoscale features with large Rossby number, *J. Phys. Oceanogr.*, *30*, 2687–2709.

Sloan, N. Q. (1996), Dynamics of a shelf/slope front: Process studies and data-driven simulations, Ph.D. thesis, Div. of Appl. Sci., Harvard Univ., Cambridge, Mass.

Watts, D. R., K. Tracey, J. Bane, and T. Shay (1995), Gulf Stream path and thermocline structure near 74°W and 68°W, *J. Geophys. Res.*, *100*, 18,291–18,312.

F. Bahr, R. C. Beardsley, K. H. Brink, M. Caruso, G. Gawarkiewicz, and J. F. Lynch, Woods Hole Oceanographic Institution, Woods Hole, MA 02543, USA. (gleng@whoi.edu)

C.-S. Chiu, Naval Postgraduate School, Monterey, CA 93943, USA.